Seismic Performance of Concrete Filled Steel Bridge Piers under High Compressive Axial Force

Kiyoshi Ono[1], Mitsuyoshi Akiyama[2], Hideki Imanishi[3] and Seiji Okada[4]

Abstract

Some methods for evaluating the seismic performance of steel bridge piers have been already proposed in previous investigations. However, almost all prior studies dealt with steel piers subjected to relatively low compressive axial forces, below $0.2N_y$ where N_y is the yield axial force. Also, in those studies, the steel piers had cross section shapes that were comparatively square. Nonetheless, reports make clear that major earthquakes such as Kobe Earthquake are likely to exert high compressive axial force onto steel piers and to other steel members such as rigid frame steel piers, arch ribs and towers of suspension bridges. Therefore, grasping the seismic performance of steel piers or steel members under high compressive axial force is a key factor in developing appropriate seismic design methodologies. In this study, cyclic loading experiments of concrete filled steel bridge piers with rectangular sections were conducted by changing the value of the compressive axial force applied to each test specimen. Based on the experiment's findings, the effects of compressive axial force on the seismic performance of concrete filled steel bridge piers with rectangular sections were investigated, along with the evaluation methods for seismic performance .

Introduction

The 1995 Kobe Earthquake caused extensive damage to highway bridges, to levels never before seen in Japan. Consequently, the seismic design specifications for highway bridges were revised in 1996 (Japan Road Association. 1996) based on greater consideration of the actual damage experience and methods of ductility design. The specifications, which had already been adapted for reinforced concrete bridge piers, were also newly applied to steel bridge piers. Following this, in 2002, more detailed seismic design methods for steel bridge piers were specified specifications (Japan Road Association. 2002b).

It is also is reported that massive earthquakes such as the Kobe Earthquake can also exert high compressive axial forces on rigid frame steel piers, arch ribs and towers of suspension bridges through varying axial force. Compressive axial force sometimes exceeds $0.5N_y$. (Here, N_y represents the yield axial force.) However, previously applied

[1] Associate Professor, Dept. of Civil Engineering, Osaka University
[2] Associate Professor, Dept. of Civil and Environment Engineering, Tohoku University
[3] Deputy Director, Kinki Regional Development Bureau, Ministry of Land, Infrastructure and Transport
[4] Bridge Design Department, IHI Infrastructure Systems Co., Ltd.

seismic evaluation methods proposed at the time were based on research and studies of steel bridge piers and steel members subjected to low compressive axial force on the level of 0.2 N_y. For hollow steel members with stiffened rectangular sections subjected to high compressive axial force on the level of 0.5 N_y, experiments and analytical studies have been conducted, resulting in proposals of new seismic performance evaluation methods. (Okada et al. 2010). However, on the other hand, studies of seismic performance of concrete filled steel bridge piers subjected to high compressive axial forces are comparatively few and there is insufficient information in this light. Furthermore, it is common in Japan for steel bridge piers to have square sections but there are also significant numbers with rectangular sections. Therefore, it is necessary to grasp the seismic performance of concrete filled steel piers with rectangular sections subjected to high compressive axial forces for proper development of better seismic evaluation methods.

In this study, cyclic loading experiments were conducted on concrete filled steel piers with rectangular section or square sections, by changing the value of the applied compressive axial forces. Based on the findings of the experiment, the seismic performance of concrete filled steel piers with rectangular section that are subjected to high compressive axial force was carefully studied along with and evaluations of seismic performance .

Outline of Experiments

(1) Test Specimens

This investigation employed six test specimens . The outline of the dimensions of the test specimens is given in Figure 1, the values of the major parameters of the test specimens are listed in Table 1. In Table 1, B_F is width of the flange and B_W is width of the web. N_{yN} is the yield axial force. R_{RN} and R_{FN} are respectively, the buckling parameters of the plate panels between longitudinal stiffeners and between stiffened plate panels. $\bar{\lambda}_N$ is the slenderness ratio parameter for the test specimen. The definitions of parameters mentioned above are identical to those stipulated in the 2002 specifications (Japan Road Association, 2002a) and are noted below. The parameters of Table 1 are calculated using nominal yield stress.

$$N_{yN} = \sigma_{yN} \times A \tag{1}$$

$$R_{RN} = \frac{b}{t}\sqrt{\frac{\sigma_{yN}}{E}\frac{12\left(1-\nu^2\right)}{4\pi^2 n^2}} \tag{2}$$

$$R_{FN} = \frac{b}{t}\sqrt{\frac{\sigma_{yN}}{E}\frac{12\left(1-\nu^2\right)}{\pi^2 k_F}} \tag{3}$$

$$\bar{\lambda}_N = \frac{1}{\pi}\sqrt{\frac{\sigma_{yN}}{E}}\frac{2h}{r} \tag{4}$$

where σ_{yN} = nominal yield stress (=315MPa); A = the sectional area of steel only sections (excluding concrete fills); h = column height (distance from the bottom of the column to the point at which horizontal load is applied); r = radius of gyration of cross section of steel members; E = Young's modulus of steel; b = width of flange or web; t = plate thickness; v = Poisson's ratio of steel ; n = number of panels; k_R, k_R = the bucking coefficients for R_{RN} and R_{FN} respectively.

The steel grade was JIS-SM490 and the plate thickness used for webs, flanges and stiffeners was 6 mm for all test specimens.

(2) Loading Conditions

Each test specimen was loaded with hydraulic jacks installed in a stiff frame. In each experiment, the specified compressive axial force shown in Table 1 was first applied to the test specimen using a vertical hydraulic jack. The values of the levels of compressive axial force, N, applied to each test specimen were 15%, 35% and 50% of yield axial force, N_{yN}, calculated by equation (1) above.

The cyclic loading pattern of horizontal displacement is schematically shown in Figure 2, where δ_{yN} is calculated by the following equation.

$$P_{yN} = \left(\sigma_{yN} - \frac{N}{A} \right) \frac{Z}{h} \tag{5}$$

$$\delta_{yN} = \frac{P_{yN} h^3}{3EI} \tag{6}$$

where I = moment of inertia of steel only sections and Z = section modulus of steel only sections.

The axial force was kept constant during the cyclic loading experiments.

Experimental Results and Comments

Figure 3 shows the examples of the horizontal load - horizontal displacement relationship (P-δ relationship). The square symbols (◆) in Figure 3 show the points where the maximum horizontal load 'P_{max}' was observed. Figure 4 (a) shows the relationship between P_{max}/P_y and N/N_y while Figure 4 (b) shows the relationship between δ_m/δ_y and N/N_y. Here, N_y is the yield axial force calculated by equation (1) although the yield stress gained from material tests is used instead of the nominal yield stress in the equation (1). P_y is the yield horizontal load calculated according to the seismic design specifications, and the yield stress gained from material tests is used in the calculation of P_y. δ_y and δ_m are respectively, the yield horizontal displacement at P_y and the horizontal displacement at P_{max}. δ_y and δ_m are determined based on the P-δ relationship obtained from the experiments. From Figures 3 and 4, it can be seen that P_{max}/P_y is little affected by N/N_y compared with

δ_m/δ_y although δ_m/δ_y decreases with as N/N_y increases. The shape of the cross section barely affects P_{max}/P_y and δ_m/δ_y.

Picture 1 indicates the out-of-plane deformation of the flange panel in the compression side at the base section when P_{max} appeared. P_{max} of the test specimen 'S15' was observed at the cyclic loop of '+8δ_y' and that of 'S-50' was observed at the cyclic loop of '+9δ_y'.As shown in Picture 1, a definite out-of-plane deformation was not observed at P_{max}. Figure 5 expresses the progress of out-of-plane deformations along the vertical direction of the flange panels at the base section after P_{max} as for test specimens 'S-15' and 'S-50'. As shown in Figure 5, the out-of-plane deformations extends rapidly after P_{max}. The same tendency shown in Picture 1 and Figure 5 was observed in all test specimens regardless of N/N_y or the shape of cross sections whether they were square sections or rectangular sections.

Evaluation Method of Seismic Performance

In the 2002 seismic design specifications included proposals for the evaluation methods for seismic performance of concrete filled steel bridge piers with square sections. These proposed evaluation methods were based on the bending moment(M)-curvature(φ) relationships (M-φ model) of steel bridge piers. The M-φ model was selected based on the previous experiment results using concrete filled steel piers; the applicable range of the M-φ model was set according to the major buckling parameters, structural details, the ratio of the axial force to the yield axial force, et al. The 2002 seismic design specifications note that the applicable range in respect of axial force does not exceed 0.2 N_{yN} and that the shape of cross sections is approximate squares. Therefore, it is not evident whether the M-φ model of the 2002 seismic design specifications can be applied to concrete filled steel bridge piers under the axial force levels of over 0.2N_{yN} or those whose cross section shape is rectangular.

Then, applicability of the M-φ model to the concrete filled steel bridge piers with rectangular section under the high compressive axial force was investigated by comparing the experimental results and the calculation results for the M-φ model in respect of P_{max} and δ_m. Figure 6 (a) shows the comparison for P_{max} and Figure 6 (b) shows the values for δ_m. In Figure 6, the filled symbols ('■' and '▲') indicate the results of test specimens under high compressive axial forces (0.35N_{yN} and 0.50N_{yN}) , the open symbols ('□' and '△') express those under low compressive axial force (0.15N_{yN}). Here, both square symbols ('■' and '□') indicate the results of test specimens with square section while the triangular symbols ('▲' and '△') express results for rectangular section specimens. For example, according to these rule, '■' would indicate the results of test specimens with square section under high compressive axial force. In addition to the experimental results in this study, the experimental results in the previous study (PWRI et al. 1997-1999) were employed in evaluations. The shape of cross sections used in the earlier study were square and the value

of the applied compressive axial force was not greater than $0.20N_{yN}$. The results of the previous study are expressed by the circular symbols '○'.

As shown in Figure 6, relatively good agreement was found between the experimental results and the results yielded by calculations using the M-φ model . The obvious influence of N/N_{yN} or the shape of cross section on the difference between the experimental results and the calculation results is not as readily seen. This indicates that the M-φ model in the 2002 seismic design specifications can be applied to the concrete filled steel bridge piers with rectangular section under compressive axial force of levels not exceeding $0.50N_{yN}$.

Conclusions

Cyclic loading experiments were conducted by changing the value of the compressive axial forces applied to concrete filled test specimens in order to gasp the effect of compressive axial force on seismic performance of concrete filled steel piers; to confirm viability of the seismic evaluation methods. The following observations were obtained from the present study regarding seismic performance of concrete filled steel bridge piers with rectangular sections subjected to high compressive axial forces.

1) P_{max}/P_y is little affected by N/N_y especially when compared to δ_m/δ_y although δ_m/δ_y decreases with higher values of N/N_y. The shape of the cross section does not appear to meaningfully affect P_{max}/P_y and δ_m/δ_y.

2) The M-φ model used in the 2002 seismic design specifications can also be applied to concrete filled steel bridge piers with rectangular sections subjected to compressive axial forces not exceeding $0.50N_{yN}$.

References

Japan Road Association (1996). *Specifications for Highway Bridges, Part V: Seismic Design* (in Japanese).

Japan Road Association (2002a). *Specifications for Highway Bridges, Part II: Steel bridges*.

Japan Road Association (2002b). *Specifications for Highway Bridges, Part V: Seismic Design*.

Public Works Research Institute of the Ministry of Construction (PWRI) and five other organizations (1997-1999). “Ultimate Limit State Design Methods for Highway Bridges Piers Subjected to Seismic Loading”, *Cooperative Research Report* (in Japanese).

Seiji OKADA, Kiyoshi ONO, Hiroaki TANIUE, Munemasa TOKUNAGA and Nobuo NISHIMURA (2010). “SEISMIC PERFORMANCE OF STIFFENED STEEL MEMBERS WITH RECTANGULAR SECTION UNDER HIGH COMPRESSIVE AXIAL FORCE”, *Doboku Gakkai Ronbunshuu A*, Vol. 66, No. 4 (in Japanese).

Table 1 Major Parameters of Test Specimens

		S-15	S-50	RW-15	RW-35	RW-50	RS-15
$N/N_{y\,\mathrm{N}}$		0.15	0.50	0.15	0.35	0.50	0.15
$\overline{\lambda_N}$		0.39	0.39	0.39	0.39	0.39	0.39
Flange, Web	R_{RN}	0.46	0.46	0.46	0.46	0.46	0.46
	R_{FN}	0.47	0.47	0.47	0.47	0.47	0.47
B_W/B_F		1.0	1.0	0.6	0.6	0.6	1.7
Yield strength of steel σ_y (MPa)		381	378	382	376	382	381
Strength of concrete σ_c (MPa)		25.8	25.6	21.2	26.3	21.1	28.0

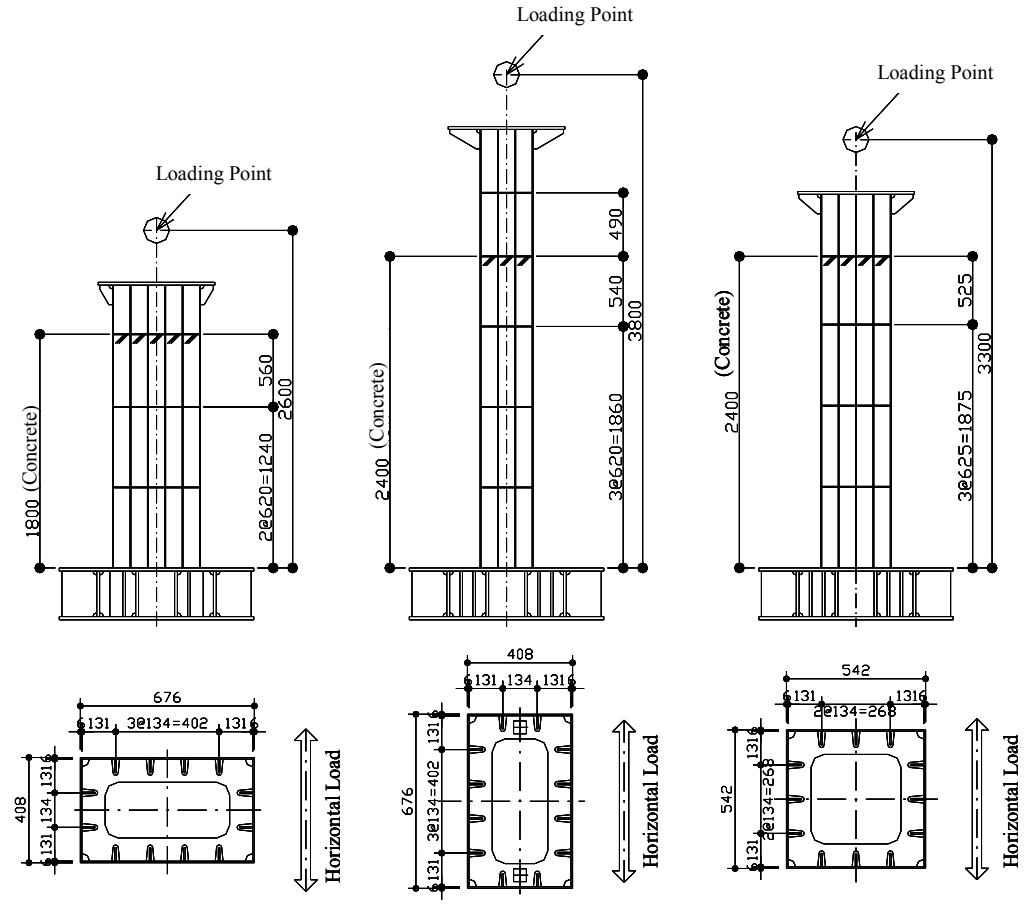

(RW-15, RW-35, RW-50) (RS-15) (S-15, S-50)

[Unit: mm]

Figure 1 Outline of Test Specimens

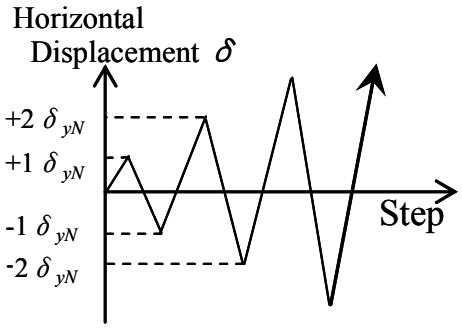

Figure 2 Cyclic Loading Patterns

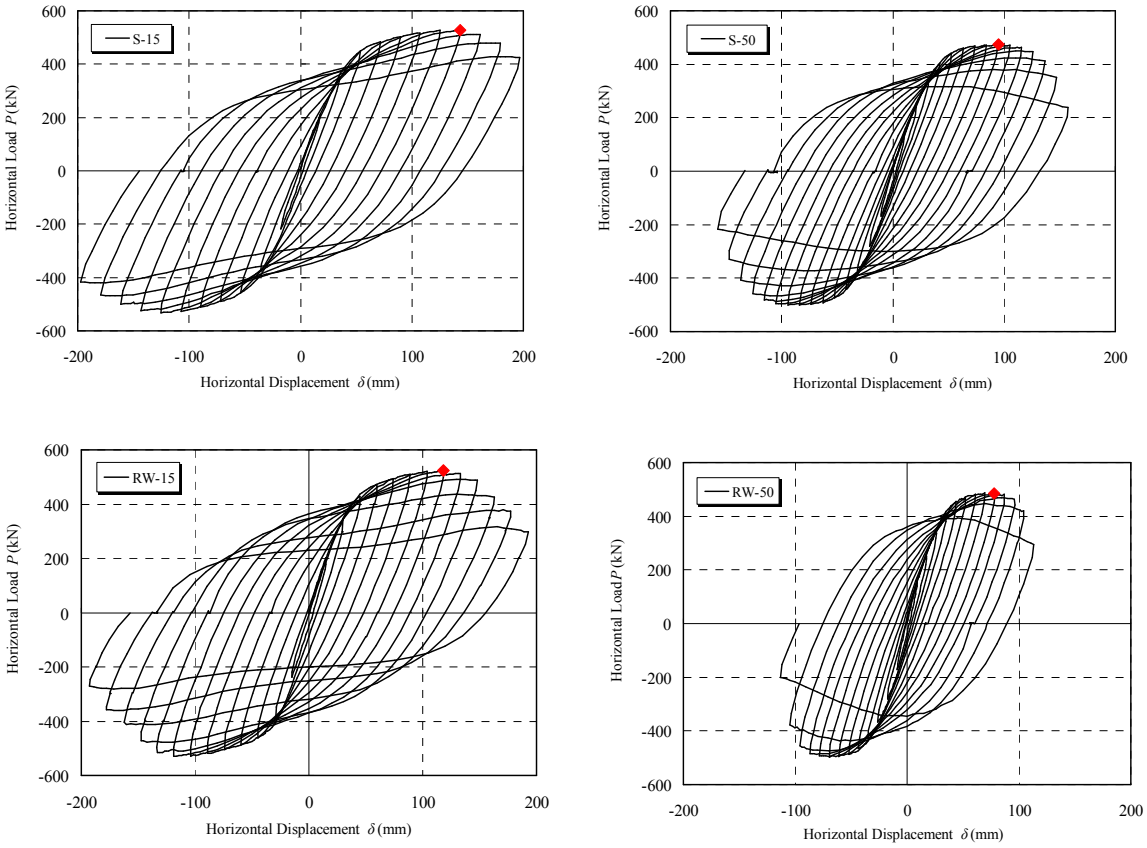

Figure 3 The *P*-*δ* Relationship

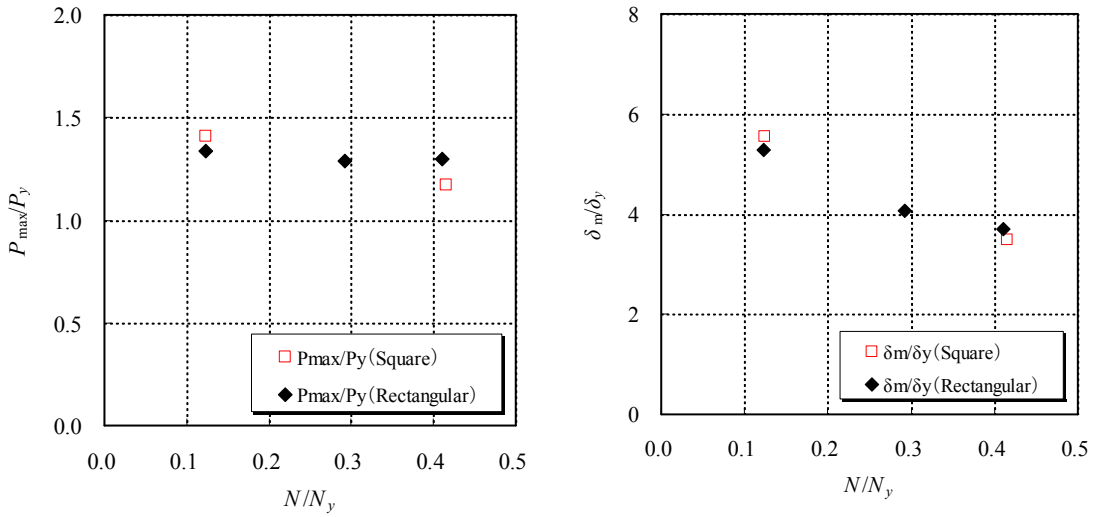

(a) P_{max}/P_y (b) δ_m/δ_y

Figure 4 Influence of N/N_y on P_{max}/P_y or δ_m/δ_y

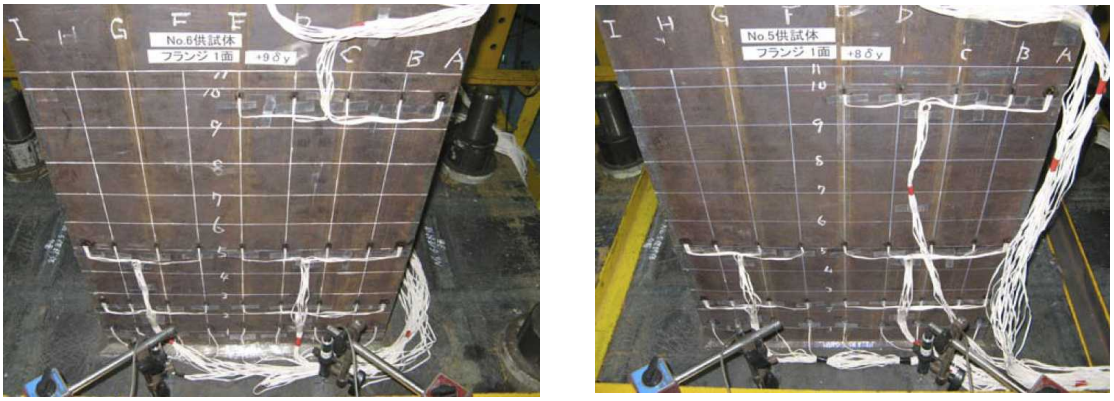

(a) Test specimen 'S-15' (b) Test specimen 'S-50'

Picture 1 Out-of-plane deformations at P_{max}

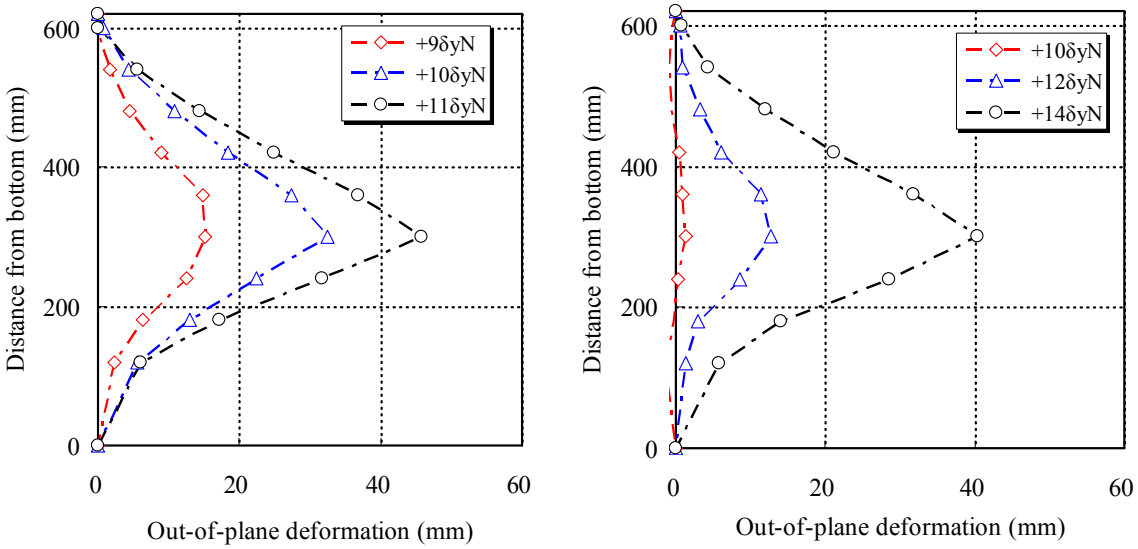

(a) Test specimen 'S-15' (b) Test specimen 'S-50'

Figure 5 Progress of out-of-plane deformation after P_{max}

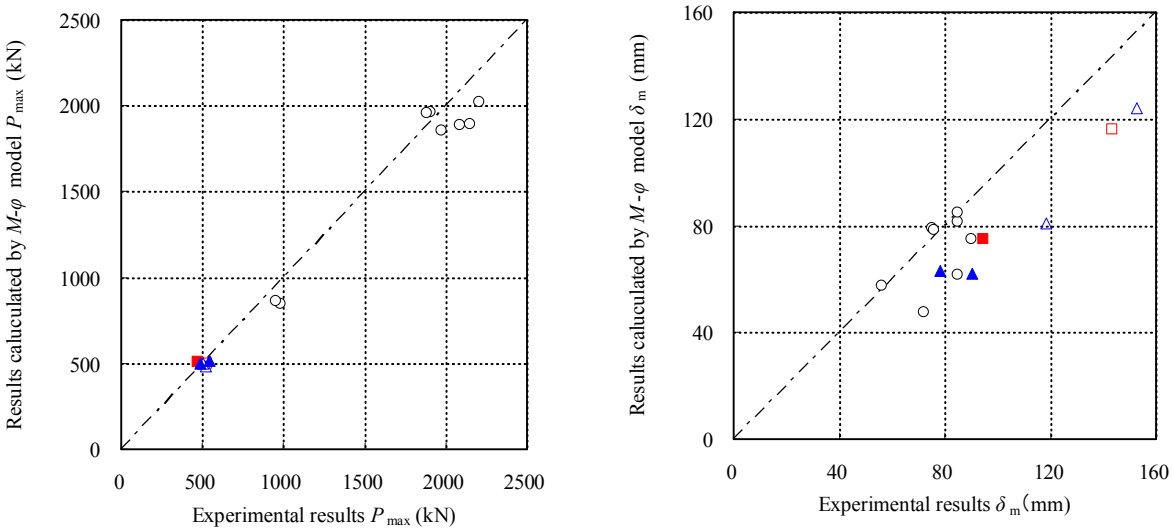

(a) P_{max}/P_y (b) δ_m/δ_y

Figure 6 Comparison of Actual Experimental Findings with the Results calculated using the *M-φ* Model